Eur. Phys. J. A **8**, 511–520 (2000)

THE EUROPEAN PHYSICAL JOURNAL A

Nuclear densities in the neutron-halo region

A. Bhagwat, Y.K. Gambhir[a], and S.H. Patil

Department of Physics, I.I.T. Powai, Bombay 400076, India

Received: 15 May 2000
Communicated by P. Schuck

Abstract. Loosely bound *Exotic Nuclei* in the neutron-halo region have very small neutron/proton separation energy implying a long tail of the last loosely bound nucleon. An accurate treatment of this tail is crucial for the description of several reaction observables. We propose, for such loosely bound *Exotic Nuclei*, a simple analytic expression for nucleon densities which incorporates correctly two basic physical requirements: a) *The asymptotic behavior* ($r \to \infty$). b) *The behavior near the center* ($r \to 0$).
The expression provides, separately, the neutron and proton densities and is suitable for the description of *Exotic Nuclei* in the neutron-halo region. In addition it provides a simple physical insight into the density in the outer (halo) region. Glauber type calculations for reaction cross-sections, using these densities have been carried out for such nuclei. The calculated cross-sections are found to be consistent with the experimental values. The calculated densities are in good agreement with the corresponding so-called experimentally deduced densities (where available) indicating the reliability of the proposed model densities.

PACS. 27.20.+n $6 \leq A \leq 19$ – 21.10.Ft Charge distribution – 21.60.-n Nuclear structure models and methods – 25.70.-z Low and intermediate energy heavy-ion reactions

1 Introduction

Most of the current nuclear physics activity is based on the heavy-ion collision experiments. With the present-day available accelerator and detection facilities, it is now possible to produce and study nuclei far away from the stability line—the so-called *Exotic Nuclei*. Highly unstable nuclei can be studied with the help of the radioactive ion beam (RIB) facility. In these investigations [1–4], the observed sudden rise in the measured interaction cross-sections in the neutron rich light nuclei, specifically while going from ^{9}Li to ^{11}Li, ^{12}Be to ^{14}Be and ^{15}B to ^{17}B has been attributed to the corresponding large increase in the nuclear mass rms radii. This fact is an indication of the sudden change in the structure of these nuclei due to the addition of the last two neutrons. The celebrated example in these investigations is the discovery of the phenomenon of *Neutron-Halo* [1] especially in ^{11}Li. The *Neutron-Halo* is qualitatively associated with the very small separation energy ($\epsilon_{\rm n}$) of the last neutron. Due to this small value of $\epsilon_{\rm n}$, the tail of its last neutron wave function and the corresponding density spreads far out from the center of the nucleus. This is understood to form what is known as *Neutron-Halo*. The *Exotic Nuclei* which lie close to the neutron/proton drip line generally have very small neutron/proton separation energy. Therefore, the correct description of their last nucleon wave function will play a crucial role in the theoretical calculations specially for observables of the scattering and reaction processes. This is akin to the situation of the very loosely bound electron in the atomic case (*e.g.* alkali atoms, negative ions). There, it was observed that it is essential to incorporate properly the correct asymptotic behavior of this last electron wave function especially for a reliable description of the photo-ionization [5] and polarizabilities [6–8]. Based on this realization, the loosely bound nucleus (*e.g.*, ^{8}B or ^{11}Li or ^{11}Be etc.) is treated as a core and a tail corresponding to the last halo neutron(s)/proton(s) having the correct asymptotic behavior governed by the separation energy of the last neutron/proton [3,9]. The so-called *experimental density* is then extracted by fitting the parameters appearing in the core density and the tail part, to reproduce the experimental data such as reaction cross-sections, transverse-momentum distribution, neutron separation energy. For example in the case of ^{11}Li the core (^{9}Li) density was taken to be of Harmonic Oscillator (HO) type and the halo neutrons were assumed to move independently in the average potential provided by the core with the same shape as that of the core density. The depth and the width of this potential were treated as parameters which were determined so as to give the right neutron separation energy (asymptotic behavior), and the density obtained yields in the Glauber model, an overall best fit to the experimental reaction cross-sections [3].

We had proposed [10,11] a simple analytic expression for the nucleon densities which incorporates correctly two basic physical requirements *the asymptotic behavior* ($r \to \infty$) *and the behavior near the center* ($r \to 0$). The

[a] e-mail: yogy@phy.iitb.ernet.in

expression uses the nucleon separation energies (*viz.* $\varepsilon_{\rm n}$ and $\varepsilon_{\rm p}$) and the charge radii as input to yield separately, the neutron and proton density distributions. The input information could be taken from the experiment where available and from the earlier published work in other cases. This density (eq. (19)) has been used [10,11] for the nuclei near the beta stability line. It yields [12] the electron scattering form factors in excellent agreement with the experiments. The resulting neutron densities are also found to be consistent [13] with the corresponding experimental observations (where available) and also with the corresponding neutron density distributions obtained from sophisticated mean-field calculations.

The loosely bound nuclei generally have large neutron/proton excess and may even lie close to the neutron/proton drip line. In addition these nuclei generally have very small nucleon separation energy and therefore a long tail, so that the correct treatment of this tail part (asymptotic behavior) is crucial. For a loosely bound nucleus, we propose [14] a density which contains explicitly an additional term describing the tail (halo). For example, for a neutron-rich nucleus (N, Z), the neutron density is written as

$$\rho_{\rm n}(r) = \rho_{\rm core}(r) + \rho_{\rm tail}(r).$$

Both the parts $\rho_{\rm core}$ and the tail $\rho_{\rm tail}$ have their correct asymptotic behavior. These expressions require the same input as before namely, the nucleon separation energies and the charge radii. The expression then provides, separately, the neutron and proton densities and also the tail part. Therefore, it renders a simple physical insight into the density in the outer (halo) region. Glauber type calculations using these densities have also been carried out for such nuclei. The calculated cross-sections are found to agree with the experiment. The calculated densities compare well with the corresponding so-called experimental densities (where available) indicating the reliability of the proposed model densities.

In section 2 the details of the ingredients of the proposed density and its final expression are presented. The results of the numerical calculations are presented and analyzed in section 3, where these are also compared with the corresponding relevant earlier studies. The paper ends with the concluding remarks.

2 Formulation

The quantum-mechanical description of atoms, molecules, and nuclei with more than two particles, encounters the difficult problem of analyzing the many-particle Schroedinger equation or its relativistic generalization. However, though the equation is very complicated in structure, it is possible to deduce some general properties of the wave functions. These properties follow from the general structure of the equation and the interaction.

2.1 General characteristics

Particularly significant are:

1) the asymptotic behavior of the wave function when one of the particles is far away from the remaining particles and
2) the behavior near the center.

We shall now discuss these in the following subsections.

2.1.1 Asymptotic behavior

The wave function in the outer region is important in the description of the interaction of the system with other particles or with external fields. We begin with a description of the asymptotic behavior of non-relativistic bound state energy eigenfunctions. The non-relativistic Hamiltonian for an N-particle system may be written as

$$H^{(N)} = \sum_{i=1}^{N} \frac{1}{2m_i} p_i^2 + \sum_{i>j}^{N} \left[V_{\rm s}(r_{ij}) + \frac{q_i q_j}{r_{ij}} \right], \qquad (1)$$

where $r_{ij} = |\mathbf{r}_i - \mathbf{r}_j|$, $V_{\rm s}(r_{ij})$ is the short-range nuclear interaction, and the Coulomb interaction $q_i q_j / r_{ij}$ dominates at large separations of the particles i, j. We consider an eigenfunction of this Hamiltonian in the center of mass frame, with eigenvalue $E_0^{(N)}$. An eigenfunction of this Hamiltonian with eigenvalue $E_0^{(N)}$, can be expanded in terms of the eigenfunctions of the $(N-1)$-particle system in its center-of-mass frame, as follows:

$$H^N \psi_0^{(N)}(1, \ldots, N) = E_0^{(N)} \psi_0^{(N)}(1, \ldots, N),$$
$$\psi_0^{(N)}(1, \ldots, N) = \sum_{n=0} f_n(\mathbf{r}) \phi_n^{(N-1)}(2, \ldots, N), \qquad (2)$$

where $\mathbf{r}$ is the position of particle 1 with respect to the center of mass of the $(N-1)$-particles $2, \ldots, N$, and

$$H^{(N-1)} \phi_n^{(N-1)}(2, \ldots, N) = E_n^{(N-1)} \phi_n^{(N-1)}(2, \ldots, N) \qquad (3)$$

with $n = 0$ representing the $(N-1)$-particle ground state. Operating by $H^{(N)}$ on $\psi_0^{(N)}$ and projecting out the n-th state one obtains

$$\left[-\frac{\hbar^2}{2m} \left(\frac{\partial^2}{\partial r^2} + \frac{2}{r} \frac{\partial}{\partial r} - \frac{L^2}{\hbar^2 r^2} \right) + \frac{q_1 Q}{r} + E_n^{(N-1)} - E_0^{(N)} \right]$$
$$\times f_n(\mathbf{r}) = -\sum_i \left\langle \phi_n^{(N-1)} \right| \sum_{j\rangle 1} \left[V_s(r_{1j}) + q_1 q_j \left(\frac{1}{r_{1j}} - \frac{1}{r} \right) \right]$$
$$\times \left| \phi_i^{(N-1)} \right\rangle f_i(\mathbf{r}), \qquad (4)$$

where $r_{1j} = |\mathbf{r} - \mathbf{r}_j|$, m is the reduced mass of particle 1, $\mathbf{L}$ is the angular-momentum operator, and

$$Q = \sum_{j>1} q_j \qquad (5)$$

is the charge of the remaining core seen by particle 1 when it is far away. In the limit of $r \to \infty$, one obtains

$$\frac{\partial^2}{\partial r^2} f_n(\mathbf{r}) = \left(\frac{2m}{\hbar^2} \right) \left[E_n^{(N-1)} - E_0^{(N)} \right] f_n(\mathbf{r}), \qquad (6)$$

so that

$$f_n(\mathbf{r}) \to \mathrm{e}^{-r[2m(E_n^{(N-1)}-E_0^{(N)})/\hbar^2]^{1/2}} \quad \text{for } r \longrightarrow \infty. \quad (7)$$

Clearly, the exponent has the smallest magnitude when $E_n^{(N-1)}$ has the lowest value and therefore the $n=0$ term dominates the asymptotic region.

In the $r \to \infty$ domain, we consider a solution of the form

$$f_0(\mathbf{r}) = \sum_{i=0} c_i r^{u-i} \mathrm{e}^{-ar} Y_l^m(\theta,\phi), \quad (8)$$
$$a = \left[\frac{2m\epsilon}{\hbar^2}\right]^{1/2},$$
$$\epsilon = E_0^{(N-1)} - E_0^{(N)}.$$

Here ℓ is the angular-momentum quantum number of the particle when it is far away from the remaining core and ϵ is its separation energy. In eq. (4) for $n=0$, the $f_0(\mathbf{r})$ term on the right-hand side is the leading asymptotic term, and for the $n=0$, $i=0$, the leading coefficient of $f_0(\mathbf{r})$ on the right-hand side is of the order of $1/r^3$ (the $1/r^2$ term vanishes because of parity). Therefore substituting eq. (8) into eq. (4), we get for the two leading terms,

$$c_i = \frac{1}{2} c_{i-1} \frac{\ell(\ell+1)-(i-u-1)(i-u-2)}{a(i-u-1)-mq_1Q/\hbar^2}, \; i=0,1. \quad (9)$$

Requiring that $c_{-1}=0$, we get

$$u = -\frac{mq_1Q}{\hbar^2 a} - 1 \quad (10)$$

and for $i=1$, we get

$$c_1 = \frac{1}{2a}(\ell-u)(\ell+1+u)c_0. \quad (11)$$

The asymptotic behavior of the wave function is then given by [15–19]

$$\psi_0^{(N)}(1,\ldots,N) \longrightarrow (r^u + dr^{u-1})\mathrm{e}^{-ar} Y_\ell^m(\theta,\phi)\, \phi_0^{(N-1)}(2,\ldots,N) \quad \text{for } r \longrightarrow \infty \quad (12)$$

$$a = \left[\frac{2m\epsilon}{\hbar^2}\right]^{1/2},$$
$$u = -\frac{mq_1Q}{\hbar^2 a} - 1,$$
$$d = \frac{1}{2a}(\ell-u)(\ell+u+1), \quad (13)$$

where $\mathbf{r}$ is the position of particle 1 with respect to the center of mass of the remaining core, m is its reduced mass with respect to the mass of the core, ϵ is its separation energy, q_1 is its charge, and Q is the charge of the remaining core. This asymptotic behavior is intuitively suggestive and understandable. The probability for a particle to be far away from the remaining system, is the highest when it has the highest energy and the remaining core has the least energy, *i.e.* the core is in its ground state. Therefore, the far away particle has an energy which is equal to the negative of the separation energy, and its asymptotic exponential behavior is given by e^{-ar} with the exponent related to the separation energy as in (eq. (8)). Furthermore, the main potential it sees is the Coulomb potential due to the remaining core which determines the leading power behavior as r^u with u related to the charges as in (eq. (13)). It should be pointed out that the leading power behavior (r^u) for the nuclear case is different for protons and for neutrons due to the dependence of u on the product of charges q_1 and Q, which is zero (as q_1 is zero) for neutrons. The next power term in the asymptotic behavior depends also on the angular momentum of the far away particle and its relative strength is given by d defined in eq. (13).

The leading term of asymptotic radial density (averaged over angles) of the particles (*e.g.*, nucleons) then takes the form

$$\rho_i(r) \longrightarrow r^{-2\alpha_i}\mathrm{e}^{(-r/a_i)} \quad \text{as } r \longrightarrow \infty, \quad (14)$$

where

$$a_i = \frac{\hbar}{2(2m\varepsilon_i)^{1/2}}, \quad (15)$$

and

$$\alpha_i = \frac{q_1Q}{\hbar}\left(\frac{m}{2\varepsilon_i}\right)^{1/2} + 1; \quad (16)$$

$i=$ n or p, $q_1=1$ for protons and $q_1=0$ for neutrons, ε_i is the corresponding nucleon separation energy, $q_1Q=0$ for neutrons and $q_1Q=Z-1$ for protons, Z being the atomic number and m is the reduced mass which for simplicity we take it to be the nucleon mass.

2.1.2 Behavior near the center

It is known [10,11,18] that the slope of the nuclear densities $\rho_i(r)$ vanishes at $r=0$, which implies that the linear term in the power series of $\rho_i(r)$ is absent. Indeed, the series should contain only the terms with even powers of r. This follows from the fact that since there are no external sources of interaction, all the derivatives of $\rho_i(r)$ (so also of the wave function Ψ_i) with respect to x, y and z exist. The presence of terms with odd powers of r would imply that some of the derivatives with respect to x, y and z are singular at the origin. This can be made plausible in terms of the Hartree-Fock equation for the wave functions;

$$-\frac{\hbar^2}{2m}\nabla^2\Psi_i(x) = \epsilon_i\Psi_i(x) - \sum_j \int V(x',x) \times \left[|\Psi_j(x')|^2\Psi_i(x) - \Psi_j^*(x')\Psi_i(x')\Psi_j(x)\right] \mathrm{d}^3x'. \quad (17)$$

Here we assume that the interaction $V(x',x)$ is a function of $|\mathbf{x}'-\mathbf{x}|$, and that the integrals exist if the wave functions are finite. Clearly, if Ψ_i exist then the first and second derivatives of Ψ_i exist (we discount the possibility that

$\nabla^2\Psi_i$ exist but the derivatives with respect to x, y and z do not exist separately). To show that the higher derivatives exist, we take the derivatives of eq. (17). For example, taking the derivative of eq. (17) with respect to x, realizing that $V(x', x)$ is a function of $|\mathbf{x}' - \mathbf{x}|$, and integrating by parts, we get

$$-\frac{\hbar^2}{2m}\nabla^2\frac{\partial\Psi_i(x)}{\partial x} = \varepsilon_i\frac{\partial\Psi_i(x)}{\partial x} - \sum_j\int V(x', x) \times\left[|\Psi_j(x')|^2\frac{\partial\Psi_i}{\partial x} + \Psi_i(x)\frac{\partial}{\partial x'}|\Psi_j(x')|^2 - \Psi_j^*(x')\Psi_i(x')\frac{\partial\Psi_j}{\partial x} - \frac{\partial\Psi_j^*(x')}{\partial x'}\Psi_i(x')\Psi_j(x) - \Psi_j^*(x')\frac{\partial\Psi_i(x')}{\partial(x')}\Psi_j(x)\right]\mathrm{d}^3\,x'. \quad (18)$$

It has already been stated that the first and second derivatives of $\Psi(x)$ exist, hence the integrals in eq. (18) exist implying thereby that the third derivatives of $\Psi(x)$ also exist. This procedure can be continued iteratively to argue that all the derivatives with respect to x, y and z of $\Psi(x, y, z)$ (so also of $\rho(r)$) exist. This of course implies that the power series for $\rho(r)$ should contain only even powers of r.

2.2 Semiphenomenological density

It is indeed encouraging that though the actual nuclear densities may have complicated structure, one can deduce some local properties at small and large distances from the center. Here we consider model nuclear densities based on these properties. We first discuss the densities for nuclei near the β-stability line. We then develop simple, analytical densities for loosely bound nuclei for which the asymptotic behavior is particularly important.

2.2.1 Nuclei near the β-stability line

We had proposed [10,11] the following simple expression for $\rho(r)$ which fulfills the above requirements namely the asymptotic behavior and behavior near the center.

$$\rho_i(r) = \frac{\rho_i^0}{1 + \left[(1 + (r/R)^2)/2\right]^{\alpha_i}\left[e^{(r-R)/a_i} + e^{-(r+R)/a_i}\right]}, \quad (19)$$

with i = n or p. The parameters ρ_n^0 and ρ_p^0 appearing in the expression of the density (eq. (19)) are determined from the normalization:

$$4\pi\int\rho_\mathrm{n}r^2\,\mathrm{d}r = N, \quad (20)$$

$$4\pi\int\rho_p r^2\,\mathrm{d}r = Z, \quad (21)$$

where $N\,(Z)$ is the total number of neutrons (protons) in the nucleus.The only remaining parameter R, is determined by requiring that the rms radius for proton density, R_p, predicted by the expression (eq. (19)) is equal to that obtained from the experimental rms charge density radius R_c, by using

$$R_\mathrm{p} \approx \left(R_\mathrm{c}^2 - 0.6\right)^{1/2}, \quad (22)$$

where 0.6 is the small correction to account for the finite size of the proton. The expression then provides separately the neutron and proton density distributions. The proposed density (eq. (19)) has been successfully used [10, 11] for the nuclei near the beta stability line. It yields [12] the electron scattering form factors in excellent agreement with the experiment. The resulting neutron densities are also found to be consistent [13] with the corresponding experimental observations (where available) and also with the corresponding neutron density distributions obtained from sophisticated mean-field calculations.

2.2.2 Loosely bound and halo nuclei

The loosely bound nuclei generally have large neutron/proton excess and may even lie close to the neutron/proton drip line. In addition these have very small nucleon separation energy and therefore a long tail, so that the correct treatment of this tail part (asymptotic behavior) is crucial. For a loosely bound nucleus, we propose a density which contains explicitly an additional term describing the tail (halo).

For example, for neutron rich nucleus (N, Z), the neutron density is written as

$$\rho_\mathrm{n}(r) = \rho_\mathrm{core}(r) + \rho_\mathrm{tail}(r). \quad (23)$$

Both the parts ρ_core and the tail ρ_tail should have their correct asymptotic behavior. Here the ρ_core (the neutron part of the core (N_c, Z)) density is given by eq. (19) in which the neutron separation energy ε_n and R correspond to the core nucleus (N_c, Z). For the neutron tail or halo part ρ_tail we take

$$\rho_\mathrm{tail} = N_0\left(\frac{r^2}{(r^2 + R^2)^2}\right)e^{-r/a_t}, \quad (24)$$

where

$$a_t = \frac{\hbar}{2(2m\varepsilon_t)^{1/2}}. \quad (25)$$

Here ε_t is the neutron separation energy of the loosely bound nucleus (N, Z) while R appearing in the expression of ρ_tail corresponds to the core nucleus (N_c, Z). The constant N_0 is to be fixed by requiring that ρ_tail corresponds to the correct number of neutrons in the tail (halo). For the proton part of the density of (N, Z), we use the expression (eq. (19)) in which the proton separation energy ε_p and R correspond to the nucleus (N, Z). This is supposed to take into account, approximately, the small differences in the proton distributions in the core (N_c, Z) and the loosely bound nucleus (N, Z).

For the case of proton rich nucleus (N, Z) the density again is composed of two parts: the core and the tail, each part having the correct asymptotic behavior. As a consequence the proton tail part will have slightly different

power dependence because of its different asymptotic behavior due to the Coulomb interaction (dependence of α on Q). It is taken as

$$\rho_{\rm tail} = N_0 \left(\frac{r^2}{(r^2+R^2)^{2+(Q/\hbar)(m/(2\varepsilon_t))^{1/2}}} \right) e^{-r/a_t}. \quad (26)$$

Here a_t is given by the same expression (eq. (25)) as before except that ε_t (and so also in eq. (23)) now corresponds to the proton separation energy of the loosely bound nucleus (N, Z). All the rest of the above description for the case of neutron-halo also holds here with neutron replaced by proton and *vice versa*.

In this picture, we therefore regard, for example, ^{8}Li (^{8}B), and ^{9}Li to be composed of ^{7}Li (^{7}Be) core and 1n (1p) and 2n neutron tail, respectively, while ^{11}Li has ^{9}Li core followed by 2n halo. Explicitly

$$^{8}\mathrm{Li} \Longleftrightarrow {}^{7}\mathrm{Li} + {}^{1}\mathrm{n},$$
$$^{8}\mathrm{B} \Longleftrightarrow {}^{7}\mathrm{Be} + {}^{1}\mathrm{p},$$
$$^{9}\mathrm{Li} \Longleftrightarrow {}^{7}\mathrm{Li} + {}^{2}\mathrm{n},$$

and

$$^{11}\mathrm{Li} \Longleftrightarrow {}^{9}\mathrm{Li} + {}^{2}\mathrm{n}.$$

2.3 Reaction studies with radioactive ion beams

The fragmentation studies in high-energy heavy-ion experiments permit to separate and then accelerate the beam of highly neutron (proton) rich unstable or halo nuclei. This secondary beam can then be used as a projectile incident on a variety of targets. These reaction studies help to extract the nuclear structure information of these unstable (very short lived) nuclei which otherwise would not have been possible. Using the measured cross-sections it is possible to extract the nuclear mass root mean square (rms) radii within the Glauber model. Infact, even the so-called experimental nuclear densities are extracted for these nuclei using the corresponding observed cross-sections, momentum distributions of the fragments and other related experimental information. A brief sketch of the Glauber model now is in order.

2.3.1 Glauber model

In the Glauber model the reaction cross-section $\sigma_{\rm R}$ is given by

$$\sigma_{\rm R} = 2\pi \int [1 - T(b)] b \, {\rm d}b \,, \quad (27)$$

where $T(b)$ is the transparency function at impact parameter b. Assuming the optical limit approximation and replacing the nucleon profile function by the average NN cross-section $\bar{\sigma}$, the transparency function $T(b)$ under the zero range limit, reduces to

$$T(b) = \exp\left[-\bar{\sigma} \int {\rm d}s \, \bar{\rho}_{\rm t}(s) \bar{\rho}_{\rm p}(\mathbf{b}-\mathbf{s}) \right]. \quad (28)$$

Here the suffix $t(p)$ refers to target (projectile) and $\bar{\rho}_i(s)$ is a z-direction integrated nucleon (sum of proton and neutron) density ρ distribution expressed as:

$$\bar{\rho}_i(s) = \int {\rm d}z \, \rho\Big(\big(s^2 + z^2\big)^{1/2} \Big), \quad (29)$$

with $s^2 = (x^2 + y^2)$. Thus the calculation of the reaction cross-section in the Glauber model requires the average NN cross-section and the density distributions of both the target and the projectile.

3 Calculations-results and discussion

We, now, present, discuss and analyse some of our results of numerical calculations using the proposed densities. The required input namely the neutron and proton separation energies $\varepsilon_{\rm n}$ and $\varepsilon_{\rm p}$ (MeV) are taken from the experiment ([20]) while the experimental charge radii ($R_{\rm c}$) are taken from [21] (where available). Otherwise these are taken from the earlier work and in the absence of it their values are based on some physical information/arguments. These together with the calculated values of the half density radius parameter R, the point proton radius ($R_{\rm p}$) are listed in table 1 for the isotopes of He, Li, Be and B considered in the present work. Similar results for the target nuclei (^{9}Be, ^{12}C and ^{27}Al) are also included in the same table.

3.1 Root mean square radii

The calculated values (calc) of the point neutron radius ($R_{\rm n}$) and the rms radius ($R_{\rm rms}$) along with the corresponding values of Tanihata and others, are listed under column labelled as Tan in table 1. It should be pointed out that the only input in our densities are the experimental nucleon separation energies ($\varepsilon_{\rm n}$ and $\varepsilon_{\rm p}$) and the charge radii ($R_{\rm c}$). In several cases the experimental nucleon separation energies and charge radii ($R_{\rm c}$) are not available and therefore these are to be taken from the earlier work or other sources. As a consequence some though small uncertainties may creep in, in the calculated results.

The inspection of the table 1 reveals that the calculated radii in general, are in good agreement with the fitted, the so-called experimental values. It is observed that the rms radii ($R_{\rm rms}$) for He isotopes are very close to those obtained in the earlier studies [2,22,23]. However, there are some differences for example the calculated neutron skin for ^{6}He (^{6}He) is $\simeq$ 0.3(0.4) fm while it is reported to be $\simeq$ 0.9(0.9) fm by Tanihata *et al.* [22] in their studies with harmonic oscillator densities. The calculated radii for Li and Be isotopes are consistent with the earlier investigations [2]. The calculated value 2.97 fm of rms radius for ^{14}Be also compares well with 3.10 ± 0.15 fm obtained in the recent investigations by Suzuki *et al.* [24]. The nucleus ^{8}B, anticipated a proton halo case, has also been studied recently by Fukuda *et al.* [9]. Describing ^{8}B as a Gaussian core plus a proton Yukawa tail and determining

Table 1. The neutron and proton separation energies (ε_n and ε_p) (MeV), the charge radii (R_c), the calculated half density radii (R), point root mean square proton (R_p) and neutron (R_n) radii, and the mass root mean square radii (R_{rms}) in fermis. The corresponding values of R_n and R_{rms} taken from [2] are also listed under Tan.

	ε_p	ε_n	R_c	R	R_p	R_n		R_{rms}	
						calc.	Tan	calc.	Tan
^{4}He	19.81	20.58	1.67[c]	0.90	1.48	1.47	1.57	1.48	1.57
^{6}He	28.19	1.86	2.46[a]	2.45	2.34	2.61	2.61	2.52	2.48
^{8}He	28.19	2.58	2.33[a]	2.25	2.20	2.59	2.64	2.50	2.52
^{6}Li	4.59	5.66	2.57[c]	1.11	2.45	2.42	2.32	2.43	2.32
^{7}Li	9.97	7.25	2.41[c]	1.63	2.28	2.55	2.27	2.44	2.33
^{8}Li	12.45	2.03	2.41[a]	1.83	2.28	2.86	2.44	2.66	2.37
^{9}Li	13.93	4.06	2.30[a]	1.74	2.17	2.72	2.39	2.55	2.32
^{11}Li	14.66	0.73	2.30[a]	1.77	2.17	3.67	3.21	3.32	3.12
^{7}Be	5.61	10.68	2.52[a]	1.31	2.40	2.09	2.25	2.27	2.31
^{8}Be	17.25	18.90	2.50[d]	2.24	2.38	2.36	–	2.37	–
^{9}Be	16.89	1.67	2.50[c]	2.22	2.38	2.93	2.40	2.70	2.38
^{10}Be	19.64	6.81	2.34[a]	2.07	2.21	2.53	2.34	2.40	2.30
^{11}Be	20.56	0.50	2.37[d]	2.15	2.24	3.12	2.78	2.83	2.73
^{12}Be	23.00	3.17	2.40[d]	2.26	2.27	2.73	2.65	2.58	2.59
^{14}Be	23.00	3.35	2.43[d]	2.30	2.30	2.95	3.22	2.70	3.16
^{8}B	0.14	13.02	2.58[b]	1.20	2.24	2.09	2.27	2.18	2.38
^{10}B	6.59	8.44	2.45[c]	1.41	2.32	2.31	–	2.32	–
^{11}B	11.23	11.45	2.42[c]	1.73	2.24	2.30	–	2.27	–
^{12}B	14.09	3.37	2.48[b]	2.08	2.36	2.56	2.42	2.42	2.39
^{13}B	15.80	4.87	2.54[b]	2.26	2.42	2.56	2.50	2.45	2.46
^{14}B	18.78	0.97	2.51[b]	2.32	2.39	3.03	2.48	2.77	2.44
^{15}B	18.20	2.77	2.50[b]	2.29	2.38	2.86	2.49	2.66	2.45
^{12}C	15.96	18.72	2.47[c]	2.17	2.35	2.32	2.35	2.33	2.35
^{27}Al	8.27	13.06	3.05[c]	2.75	2.95	2.87	–	2.91	–

([a]) Ref. [1], ([b]) ref. [2], ([c]) ref. [16], ([d]) see text.

the parameters of their model through the least-square fit to the observed reaction cross-sections at lower projectile (^{8}B) energies (32–60 A MeV) on Be, C and Al targets, obtained the value 2.53 ± 0.03 (2.31 ± 0.05) fm for point proton (neutron) radius and 2.45 ± 0.10 fm for the rms radius. They found appreciable variations in these values when compared with the earlier experimental and theoretical investigations. The present calculated values are in fair agreement with their values and also with those reported in [2]. It is fair to say that our calculated values, overall, are in good agreement with the corresponding fitted ones, the so-called experimental, values.

The calculated rms (R_{rms}) radii for ^{6,8}He, ^{8,10}Li, ^{9,11}Be and ^{8,14}B nuclei are arranged in table 2. The corresponding values of the core and the tail (halo) parts are also given in the same table together with their respective fitted ones, the so-called experimental values (expt) where available. The results indeed are similar to the earlier work [3] though the calculated values of R_{rms} for ^{6}He, ^{8,11}Li, ^{9,11}Be and ^{14}B are relatively larger. We notice that the experimental (fitted) R_{rms} of the core (^{9}Li) in ^{11}Li is significantly larger (2.61 ± 0.10) as compared with (2.32 ± 0.02) of the ^{9}Li nucleus while in our case there is hardly any difference between the two.

3.2 Density distributions

We now present and analyze the density distributions of ^{8}B, ^{10}B, ^{11}Li and ^{11}Be. The reason for selecting these nuclei is that for them some experimental density distributions are available. The density distribution of ^{8}B nucleus has been deduced recently by Obuti *et al.* [25] and by Fukuda *et al.* [9]. Obuti *et al.* described ^{8}B as a ^{7}Be core plus a single proton. The core (^{7}Be) density distribution, assumed to be of the Woods-Saxon shape with diffuseness parameter to be 0.65 fm, was determined so as to fit the experimental ^{7}Be + C cross-section. The single-proton (tail) wave function and hence the density were obtained by solving the Schroedinger equation with the Woods-Saxon and Coulomb potential so as to have the correct proton separation energies corresponding to $1p$, $2s$ and $1d$ orbitals. The core and the tail parts were added to get the total density distribution. Similar analyses were carried out for ^{8}Li assuming it to be composed of ^{7}Li core and a single neutron. Both the core (^{7}Li and ^{7}Be) distributions were found to be almost identical. The density distributions of both ^{8}B and ^{8}Li are very similar but the tail of ^{8}B extends to a much larger distance due to its small (0.137 MeV) proton separation energy (ε_p), the corresponding (neutron separation energy) value for ^{8}Li being 2.0 MeV. Our results shown in figs. 1 and 2 agree with

Table 2. The calculated root mean square radii $R_{\rm rms}$ (in fm) of loosely bound nuclei along with the $R_{\rm rms}$ values of the respective core and tail parts. The corresponding values taken from the earlier work are also listed under expt.

Nucleus		calc.	expt.	Nucleus		calc.	expt.
^{6}He	core	1.48	1.57±0.04	^{8}He	core	1.48	1.57±0.04
	halo	3.39	–		halo	3.00	–
	total	2.52	2.48±0.03		total	2.50	2.52±0.03
^{8}Li	core	2.44	2.33±0.02	^{11}Li	core	2.55	2.61±0.10*
	halo	3.85	–		core	2.55	2.50±0.10$^{\#}$
	total	2.66	2.37±0.02		halo	5.61	4.80±0.8*
					halo	5.61	4.80±0.8$^{\#}$
					total	3.32	3.12±0.30*
					total	3.32	3.05±0.30$^{\#}$
^{9}Be	core	2.37	–	^{11}Be	core	2.40	2.30±0.02
	halo	3.39	–		halo	6.61	–
	total	2.52	2.38±0.01		total	2.83	2.73±0.05
^{8}B	core	2.27	2.31±0.02	^{14}B	core	2.45	2.46±0.12
	halo	2.59	–		halo	5.48	–
	total	2.25	2.38±0.04		total	2.77	2.44±0.06

(*) Ref. [3] (1p halo neutron orbitals).

(#) Ref. [3] (2s halo neutron orbitals).

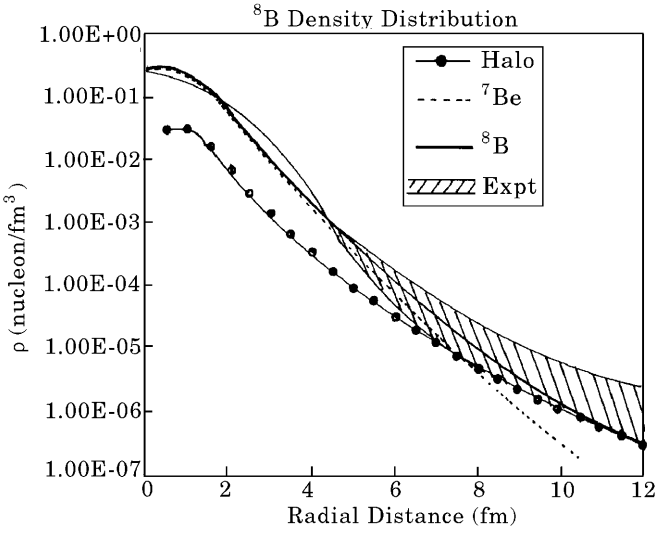

Fig. 1. The calculated density distribution for ^{8}B. The core (^{7}Be) and the halo (single proton) parts are also shown seperately. The experimental density distribution taken from [9] is also shown.

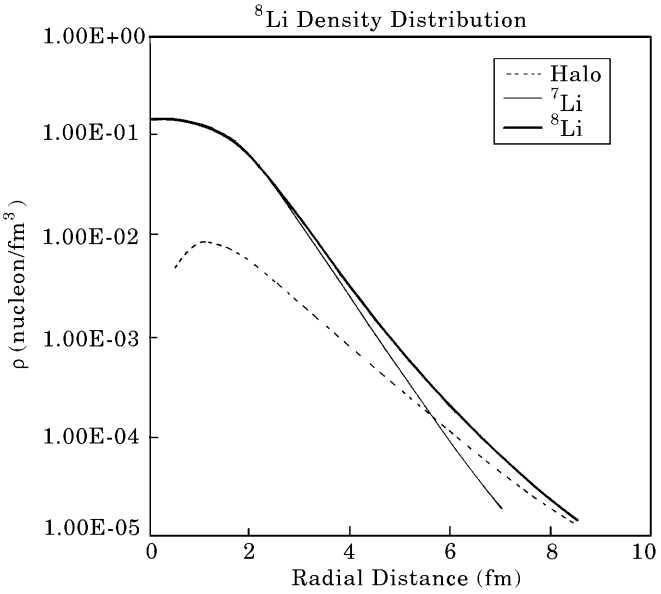

Fig. 2. The calculated density distribution for ^{8}Li. The core (^{7}Li) and the halo (single neutron) parts are also shown seperately.

these observations. Fukuda *et al.* [9] considered ^{8}B as a Gaussian core plus a proton Yukawa tail and determining the parameters of their model through the least squares fit to the observed reaction cross-sections at lower projectile (^{8}B) energies (32–60 A MeV) on Be, C and Al targets, obtained its density distribution. This is shown in fig. 1 along with the present calculated density distribution for ^{8}B. Clearly the distributions closely resemble each other.

The density distribution of ^{10}B was investigated by Cichocki *et al.* [26] in their study of electron scattering from ^{10}B. In particular they measured in the (e, e′) reaction on ^{10}B the pure isovector M3 form factor of 1.74 MeV excitation, the Fourier transform of which yields the $1p_{3/2}$ single nucleon (proton) wave function. The $1p_{3/2}$ density (normalized to shell occupancy of three protons) obtained from the Fourier-Bessel analysis of this M3 form factor is shown in fig. 3 (shaded band labelled as $1p_{3/2}$). The curves A, B and C are obtained by using a different parameterization of the contribution for C2 multipoles (quadrupole) of the elastic and 6.025 MeV inelastic form factors. The curve A is obtained by using the observed value of 8.472 fm^2 in the simple $1p$-shell model expression of the C2 form factor. In a way the curves A and C which use different parameter-

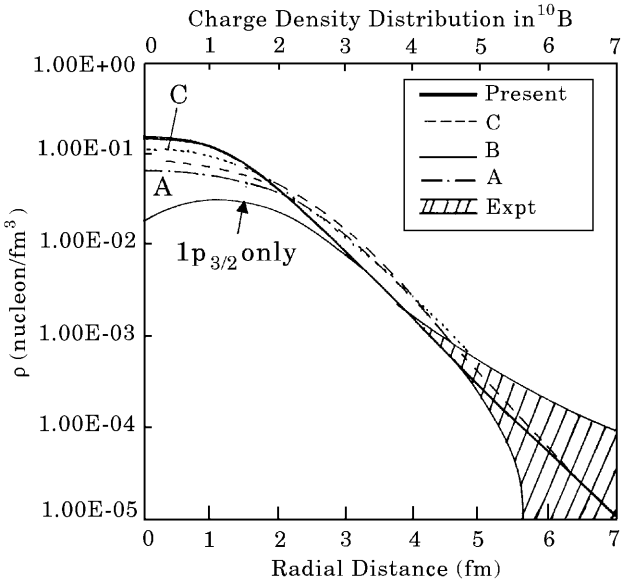

Fig. 3. The calculated point proton density distribution for ^{10}B marked 'Present'. For explanation of the labels A, B, C see text. The experimental density distribution taken from [26] is also shown.

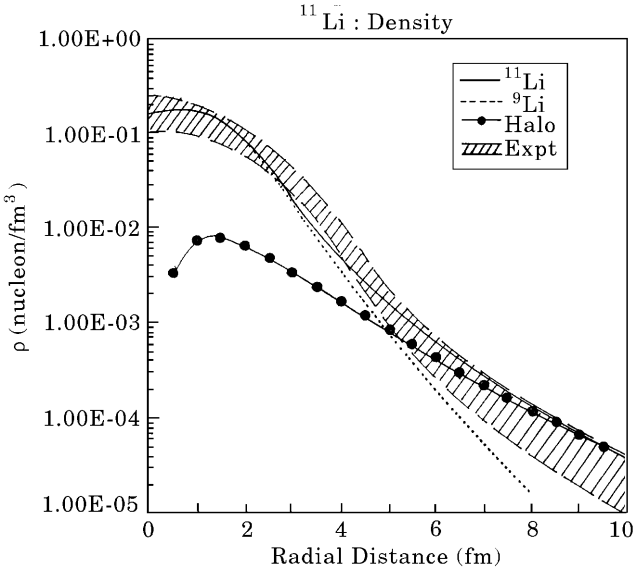

Fig. 4. The calculated density distribution for ^{11}Li. The core (^{9}Li) and the halo (two neutrons) are also shown seperately. The experimental density distribution taken from [3] is also shown.

izations correspond to lower and upper bounds on the C2 component. Our calculated model proton density is also shown which fits the curves reasonably well. The tail part essentially lies within the shaded area.

The calculated density distribution for ^{11}Li is shown in fig. 4. The core (^{9}Li) and the two neutron-halo parts are also shown. The intuitive neutron-halo structure of ^{11}Li is amply clear from the figure. The so-called experimental density of ^{11}Li obtained by Tanihata [3] is also shown. Tanihata *et al.* [3] regarded ^{11}Li to be composed of ^{9}Li core plus two halo neutrons. The core was assumed to have harmonic oscillator density with four nucleons in the $1s$ orbital and the remaining one proton and four neutrons occupying $1p$ orbital. The halo neutrons were assumed to move independently in the potential provided by this core having the shape (harmonic oscillator) of the core density. The two neutron density (halo part) was added to the core part to get the total density for ^{11}Li. The depth (width of the oscillator potential) and the binding energy (neutron separation energy) were treated as parameters for the calculation of the halo part and were fixed by fitting the observed cross-sections. Two orbitals $2s$ and $1p$ were considered for the halo neutrons. The fitted width parameter gave larger size ($R_{\rm rms}$) *viz.* $2.50 \pm 0.10 (2.61 \pm 0.10)$ for the $1p$ ($2s$) orbitals, for the core (^{9}Li). As mentioned before the corresponding present calculated value is 2.55 fm. The density distributions for ^{11}Li by Tanihata *et al.* [3] for both $2s$ and $1p$ orbitals were almost identical. This is not difficult to understand as the leading part of the asymptotic behavior of the tail part is independent of the orbital angular momentum and it appears only in the next order (see eqs. (12), (13)). Clearly, the calculated density of ^{11}Li shown in fig. 4, agrees well with the experiment (deduced by Tanihata *et al.* [3]) and lies within the experimental uncertainties. This indeed is gratifying in view of the very simple analytic form of the proposed density. It indicates the accuracy of the proposed form of density.

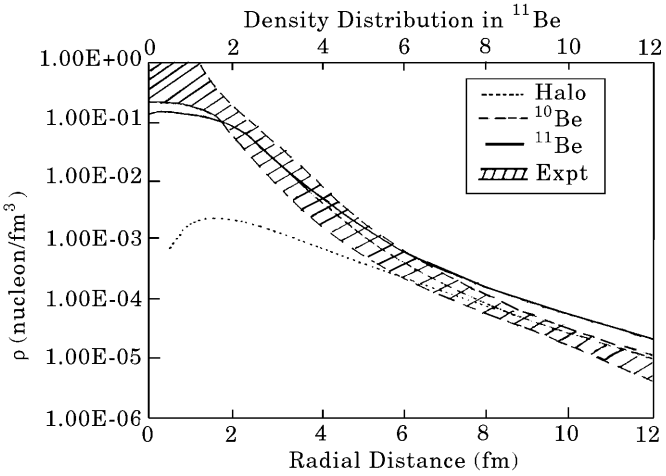

Fig. 5. The calculated density distribution for ^{11}Be. The core (^{10}Be) and the halo (single neutron) are also shown seperately. The experimental density distribution taken from [3] is also shown.

The density distribution of ^{11}Be was obtained by Fukuda *et al.* [27], assuming it to be composed of a core density of Gaussian shape and a single neutron Yukawa tail. The parameters were obtained through the best fit to the observed reaction cross-sections for 790 A MeV ^{11}Be incident on ^{12}C and ^{27}Al targets, in the Glauber model. This density shown in fig. 5 by shaded part compares well with the present calculated model density for ^{11}Be.

Table 3. The calculated reaction cross-sections ($\sigma_{\rm calc}$ (mb)) in the Glauber model using the present densities at 790/800 A MeV incident energy on ^{9}Be, ^{12}C and ^{27}Al targets, along with the corresponding experimental values.

Target	^{9}Be		^{12}C		^{27}Al	
	$\sigma_{\rm calc}$	$\sigma_{\rm expt}$	$\sigma_{\rm calc}$	$\sigma_{\rm expt}$	$\sigma_{\rm calc}$	$\sigma_{\rm expt}$
Projectile						
^{4}He	461	485 ± 4	462	503±5	745	780±13
^{6}He $\Longrightarrow$ ^{4}He+2n	678	672±7	703	722±6	1084	1063±8
^{8}He $\Longrightarrow$^{4}He+4n	767	757±4	780	817±6	1184	1197±9
^{6}Li	672	651±6	695	688±10	1060	1010±11
^{7}Li	720	686±4	734	736±6	1103	1071±7
^{8}Li $\Longrightarrow$^{7}Li+1n	795	727±6	814	768±9	1217	1147±14
^{9}Li $\Longrightarrow$^{7}Li+2n	815	739±5	823	796±6	1222	1135±7
^{11}Li $\Longrightarrow$ ^{9}Li+2n	1025	981±20	1068	1047±40	1605	–
^{7}Be	688	682±7	699	738±9	1059	1050±17
^{8}Be	743	–	744	–	1107	–
^{9}Be $\Longrightarrow$ ^{8}Be+1n	834	755±6	848	806±9	1263	1174±11
^{10}Be $\Longrightarrow$ ^{8}Be+2n	814	755±7	806	813±10	1191	1153±16
^{11}Be $\Longrightarrow$ ^{10}Be+1n	947	878±10	969	942±8	1463	1382±25
^{12}Be $\Longrightarrow$ ^{10}Be+2n	925	873±22	922	927±18	1349	1305±31
^{14}Be $\Longrightarrow$ ^{12}Be+2n	1021	–	1021	1139±90	1479	–
^{8}B $\Longrightarrow$^{7}Be+1p	710	731±15	712	784±14	1077	1106±32
^{10}B	799	–	794	–	1179	–
^{11}B	815	–	799	–	1182	–
^{12}B $\Longrightarrow$ ^{11}B+1n	873	814±9	859	866±7	1262	1250±15
^{13}B $\Longrightarrow$^{11}B+2n	904	890±17	885	883±14	1293	1233±28
^{14}B $\Longrightarrow$^{13}B+1n	998	860±31	997	929±26	1470	1264±43
^{15}B $\Longrightarrow$ ^{13}B+2n	1007	925±120	996	962±160	1448	1175±180

Table 4. The calculated reaction cross-sections ($\sigma_{\rm calc}$ (mb)) in the Glauber model using the present densities at various incident projectile energies (MeV) on ^{9}Be and ^{12}C targets, along with the corresponding experimental values.

Projectile	^{11}Li			^{14}Be		
	Energy	$\sigma_{\rm calc}$	$\sigma_{\rm expt}$	Energy	$\sigma_{\rm calc}$	$\sigma_{\rm expt}$
Target						
^{12}C	400 A	922	989±21			
	790 A	1068	1047±14	790 A	1066	1139±90
	800 A	1070	1056±14			
				850 A	1068	1082±34
^{9}Be	400 A	861	911±20			
	800 A	1026	981±20			

3.3 Reaction cross-sections

The reaction cross-sections are calculated in the Glauber model for 790 A (MeV) He-, Li-, Be-, and B-isotopes as projectiles incident on ^{9}Be, ^{12}C and ^{27}Al targets using these densities. These are listed in table 3 along with the corresponding experimental values taken from [1,2]. The calculations agree well with the corresponding experimental values. However, small ($\leq 7\%$) differences do appear at some places. Next we analyze the energy dependence of the reaction cross-sections in the Glauber model. The calculated cross-sections using the present densities at different energies for projectiles (^{11}Li,^{14}Be) incident on ^{9}Be and ^{12}C targets are arranged in table 4 together with the corresponding experimental values [3]. Here also the calculated results are in good agreement with the experimental values. We may conclude that the present calculated results are indeed satisfactory. This is important as it demonstrates the reliability of the proposed densities.

In summary, we reiterate that overall, our simple analytic expressions for nuclear densities with the correct asymptotic behavior provide a useful and accurate (reasonable) description of the nuclear densities.

The financial support from the Department of Science and Technology (DST), Government of India (Project No. SP/S2/K08/95) is gratefully acknowledged.

References

1. I. Tanihata *et al.*, Phys. Rev. Lett. **55**, 2676 (1985).
2. I. Tanihata *et al.*, Phys. Lett. B **206**, 592 (1988).
3. I. Tanihata *et al.*, Phys. Lett. B **287**, 307 (1992).
4. I. Tanihata, J. Phys. G: Nucl. Part. Phys. **22**, 157 (1996), Prog. Part. & Nucl. Phys. **35**, 505 (1995).
5. S.H. Patil, Phys. Rev. A **46**, 3855 (1992).
6. S.A. Adelman, A. Szabo, J. Chem. Phys. **58**, 687 (1973).
7. G. Lamm, A. Szabo, J. Chem. Phys. **67**, 5942 (1978).
8. S.H. Patil, K.T. Tang, J. Chem. Phys. **106**, 2298 (1997).
9. M. Fukuda *et al.*, Nucl. Phys. A **656**, 209 (1999).
10. Y.K. Gambhir, S.H. Patil, Z. Phys. A **321**, 161 (1985).
11. Y.K. Gambhir, S.H. Patil, Z. Phys. A **324**, 9 (1986).
12. Y.K. Gambhir, P. Ring, H.De Vries, Europhys. Lett. **10**, 219 (1989).
13. G. Lalazissis, C.P. Panos, M.E. Grypeos, Y.K. Gambhir, Z. Phys. A **357**, 429 (1997).
14. A. Bhagwat, Y.K. Gambhir, S.H. Patil, to be published.
15. E.N. Lassettre, J. Chem. Phys. **43**, 4475 (1965).
16. J. Katriel, E.R. Davidson, Proc. Nat. Acad. Sci. (U.S.A.) **77**, 4403 (1980).
17. A. Ahlrichs, M. Hoffmann-Ostenhoff, T. Hoffmann-Ostenhoff, J.D. Morgan, Phys. Rev. A **23**, 2106 (1982).
18. D. Berdichevsky, U. Mosel, Nucl. Phys. A **388**, 205 (1982).
19. S.H. Patil, J. Phys. B **22**, 2051 (1989).
20. G. Audi, A.H. Wapstra, Nucl. Phys. A **565**, 1 (1993); **565**, 66 (1993).
21. C.W. de Jager, H. de Vries, C. de Vries, At. Data Nucl. Data Tables **36**, 495 (1987).
22. I. Tanihata *et al.*, Phys. Lett. B **289**, 261 (1992).
23. A.A. Korsheninnikov *et al.*, Nucl. Phys. A **617**, 45 (1997).
24. T. Suzuki *et al.*, Nucl. Phys. A **655**, 313 (1999).
25. M.M. Obuti *et al.*, Nucl. Phys. A **609**, 74 (1996).
26. A. Cichocki *et al.*, Phys. Rev. C **51**, 2405 (1995).
27. M. Fukuda *et al.*, Phys. Lett. B **268**, 339 (1991).